Phase-locking Josephson junctions arrays

M. Cirillo[a)]
Dipartimento di Fisica and Unità INFM, Università di Roma "Tor Vergata", I-00133 Roma, Italy

G. Rotoli
Dipartimento di Energetica and Unità INFM, Università di L'Aquila, I-67040 L'Aquila, Italy

F. Mueller, J. Niemeyer, and R. Poepel
Physikalisch-Technische Bundesanstalt, Bundesallee 100, D-38116 Braunschweig, Germany

We demonstrate that a large area Josephson junction oscillating in the fluxon oscillator mode can be synchronized to other large junctions and simultaneously pump, by emitted radiation, a small area junction. We study the synchronization of the oscillations of the long junctions as a function of relevant experimental parameters such as bias current and stripline coupling characteristics. Experimental results obtained on coupled series arrays of Josephson junctions designed on the basis of our calculations are presented. We have fabricated coupled arrays containing each up to 1500 junctions in order to estimate the usefulness of our calculations for voltage standard devices. © *2001 American Institute of Physics.* [DOI: 10.1063/1.1402662]

I. INTRODUCTION

The reliable fabrication technology of Josephson junctions based on all refractory materials has allowed the realization of several successful integrated superconducting circuits and devices. A limit has been established, using a multiwasher device, for the sensitivity of dc-superconducting quantum interference devices[1] and reliable voltage standard devices are nowadays used for calibrations up to 10 V.[2] A fully integrated receiver system is presently being developed:[3] this device includes a long Josephson junction (LJJ) biased on Fiske and Eck steps[4] as a pumping device of the superconductor–insulator–superconductor mixer element.

Along with the success achieved in superconducting devices, the well established fabrication process has opened perspectives in the study of the physics of complex tunnel junction-based systems such as multistacked junctions,[5–7] large planar arrays,[8] macroscopic evidence of quantum levels,[9] and complex bidimensional dynamics.[10]

Recently, interesting phenomena concerning the dynamics of two-dimensional arrays based on trilayer Josephson junctions have been reported.[8] These experiments have confirmed that the problem of the coherence of nonlinear systems is intriguing, stimulating, and potentially very useful for applications. Indeed, several publications were devoted to the study of phase-locking phenomena in Josephson systems in the past two decades; beside the interest for the practical realization of Josephson voltage standards,[11] work was also devoted to the study of the locking between planar distributed oscillators.[12–16]

In the present article, we investigate by numerical simulations and experiments phase-locking phenomena in hybrid Josephson junctions systems; the systems investigated are hybrid in the sense that they contain both long junctions and small area Josephson junctions (SJJ). We investigate the ranges of stability of the phase-locking between a LJJ oscillator and a small junction and the possibility of phase locking an array of LJJ oscillators to an array of SJJ; we also report on experiments that have been thought and performed on the basis of our calculations. We recall here that the physical dimensions of Josephson tunnel junctions are considered "long" or "short" depending on their size relative to the penetration depth $\lambda_j = \sqrt{\Phi_0/2\pi\mathcal{I}\mathcal{L}}$ where $\Phi_0 = 2.07 \times 10^{-15}$ Wb is the flux quantum; $\mathcal{I}$ and $\mathcal{L}$ represent, respectively, the supercurrent density and inductance per unit length of the junctions.

In Sec. II, we describe the capacitive coupling model at the basis of our simulations and present the results obtained for the long Josephson oscillators coupled to small junctions. In Sec. III, we show the numerical results obtained for the coupling of two arrays; in Sec. IV, we present experimental data that have been obtained on real Josephson junctions arrays. In Sec. V, we conclude the article by discussing the possible impact of our results on voltage standard research and superconducting electronics.

II. THE MODEL

The model that we intend to investigate consists in its simplest form of two long Josephson junctions coupled each at one end to a small area junction which is the system shown in Fig. 1. Before analyzing the full circuit equations for this model, we will go through two preliminary steps. Let us consider first the circuit equations obtained from Fig. 1 considering only one LJJ coupled via the capacitor C_1 to the SJJ above it and neglect the rest of the circuit: shorting node 1 with 2 and node 3 with 4 as shown by the dashed vertical lines. The Kirchoff laws give

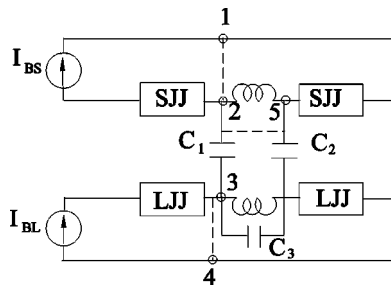$$C_1(\dot{v}_s - \dot{v}_L) = J_s, \tag{1}$$

FIG. 1. The capacitively coupled Josephson junctions systems investigated are shown. The dashed lines indicate shorting paths generating subcircuits that we analyzed before considering the whole system.

$$C_1(\dot{v}_L - \dot{v}_s) = J_L, \tag{2}$$

where C_1 is the coupling capacitor between small and long junctions; v_s and v_L are, respectively, the voltages of small and long junction (at the end points labeled 1 and 2 in the Fig. 1). J_s and J_L are currents from Josephson elements which can be written as:

$$J_s = -C_s\dot{v}_s - G_s v_s - I_s \sin\varphi_s + I_s^b, \tag{3}$$

$$J_L = -\mathcal{C}(\Delta x/2)\dot{v}_L - \mathcal{G}(\Delta x/2)v_L - \mathcal{I}(\Delta x/2)\sin\varphi_L$$
$$+ \mathcal{I}^b(\Delta x/2) + \frac{\Phi_0}{2\pi\mathfrak{L}}\frac{\partial^2\varphi_L}{\partial x^2}(\Delta x/2), \tag{4}$$

where, C_s, G_s, and I_s are, respectively, the capacitance, the conductance, and Josephson supercurrent of the small junction, while $\mathcal{C}$ and $\mathcal{G}$ are, respectively, the capacitance and the conductance per unit length. Finally Δx is the length of the last element of long junction and I_s^b and $\mathcal{I}^b$ are, respectively, the bias current of small junction and bias current per unit length of long junction (normalized to the maximum Josephson supercurrent). In this article, we will often set $\gamma \equiv I_s^b$ for typographic convenience.

The system of differential Eqs. (1)–(4) has been integrated, after discretizing the long Josephson junction in N sections, by a Bulirsh–Stoer routine. We chose for the long junction a normalized length $l = 3$ with $N = 60$ sections. We tested that the results were not dependent upon N making runs with different values of N. We note that, for simplicity, we assumed the bias current was uniformly distributed inside the long junctions. However, as far as fluxon oscillations are concerned, for the lengths and the loss parameter, that we will consider, there is not much difference in the fluxon dynamics between overlap (uniform) or inline (boundary) bias current injection. Thus, the internal dynamics of the LJJ was accounted for by an equation similar to Eq. (4) with the left-hand side set to zero. At the uncoupled ends of the LJJs, we imposed open circuit boundary conditions.

In the first set of simulations in which we only coupled a single long junction to a single small junction, this latter had a normalized length $l_s = 0.05$ corresponding to one section of long junction model. Current densities are assumed equal in the long and small junction and in all simulations the time is normalized to the plasma frequency $\omega_j = \sqrt{2\pi\mathcal{I}/\Phi_0\mathcal{C}}$. In order to avoid pumping of the small junction below its plasma
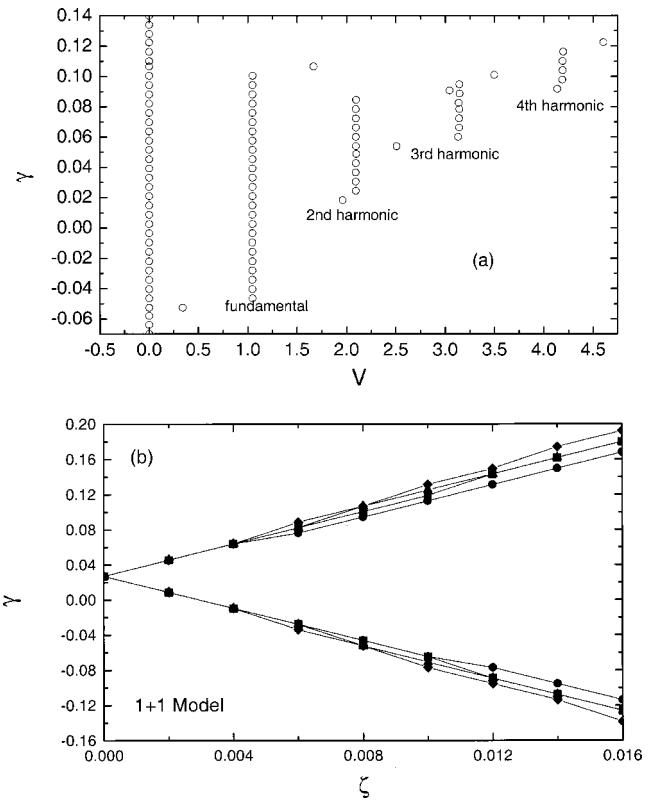

FIG. 2. (a) Current–voltage characteristics of a point Josephson junction pumped by the power emitted by a long Josephson junction biased on the first ZFS and (b) dependence of the amplitude of the first Shapiro step shown in (a) upon the coupling parameter are shown. Different symbols are relative to distinct bias points.

frequency, its capacitance was chosen slightly larger than that of a unit section of the long junction. For both junctions, we fixed a loss parameter $\alpha = 1/\sqrt{\beta_c} = G_s\sqrt{\Phi_0/2\pi C_s I_s} = 0.025$.

The results of the integrations were analyzed in terms of voltage and phase versus time plots, but we believe that the clearest way to display the results is the plot of the current–voltage characteristics of the junctions. The basic coupling scheme described by the system of Eqs. (1)–(4) was investigated in Ref. 17 and it was found that the relevant parameter for the capacitive loading is the normalized quantity $\zeta = C_1/\mathcal{C}\lambda_j$. In Fig. 2(a), we show the result of an integration obtained from fixing all the parameters of the coupled system as described in the previous paragraph and the coupling parameter $\zeta = 0.008$. Under these conditions, the single fluxon shuttling oscillations in the long junction generated a "natural" oscillation frequency which gave rise to a voltage $V_s \cong 2$ and very stable zero-field steps (ZFS)[12,13] in the current–voltage characteristics. In Fig. 2(a), we report part of the current–voltage characteristic of the "small" junction where we can see Shapiro steps in the current–voltage characteristics obtained for a dc bias point of the long junction model determined by $\mathcal{I}^b = 0.25$. The phase locking between the junctions is very stable and the first Shapiro steps (which cross the zero current axis) have an amplitude which goes up to 15% of the Josephson critical current.

In Fig. 2(b), we show the obtained amplitude of the first Shapiro step of the small junction obtained sweeping the

coupling parameter from zero up to 0.016 for three different values of the dc bias current of the long junction which are, respectively 0.15, 0.3, and 0.45 for circles, squares, and triangles; all the other parameters were like in Fig. 2(a). Figure 2(a) shows that for the higher values of the coupling parameter, the amplitude of the step goes up to 30% of the maximum Josephson supercurrent and that the amplitude of the step is not critically dependent upon the value of the bias current in the long junction. This configuration and such step amplitudes would be enough to provide a stable dc bias point on the Shapiro step for voltage standard oriented applications. Note that the points on the zero-voltage axis in Fig. 2(a) represent the Josephson current that in this case was depressed of 10% of its maximum value.

III. COUPLED ARRAYS

We analyze now the circuit shown in Fig. 1 in two situations more complex than that reported in Sec. II. We will first consider the circuit obtained removing the vertical shorting path (dashed line shorting node 3 to 4 in Fig. 1) in the LJJs series connection and shorting nodes 2 and 5 by means of the path indicated by the horizontal dashed line: thus, the two long junctions are coupled to the small junction on the left-hand side while the small junction on the right-hand side is shorted out. Successively, we will consider the dynamics of the whole circuit (removing all the shorting paths). In the first case investigated here, two coupled long junctions are pumping by means of the capacitors C_1 and C_2 a single small junction and the equations that we integrate are:

$$C_1(\dot{v}_{L1}-\dot{v}_s)+C_3(\dot{v}_{L1}-\dot{v}_2)=J_{L1}, \tag{5}$$

$$C_3(\dot{v}_{L2}-\dot{v}_{L1})+C_2(\dot{v}_{L2}-\dot{v}_s)=J_{L2}, \tag{6}$$

$$C_1(\dot{v}_s-\dot{v}_{L1})+C_2(\dot{v}_s-\dot{v}_{L2})=J_s. \tag{7}$$

Here again, J_s, J_{L1}, and J_{L2} are currents from Josephson elements that can be written as in Eqs. (3) and (4) and C_3 is the coupling capacitor between two long junctions. In the simulations, we have neglected the effect of the inductors connecting the two long junctions: the effect of these inductors, from the point of view of the modeling, is to provide a series dc connection between the junctions. At high frequency, in practical experimental situations, we have estimated that the values of the inductances connecting the junctions are so high that most of the rf current goes through the capacitor. We started the integration in the two LJJs with initial data generating single flux-quanta oscillations in both the junctions with an arbitrary position. The same bias current was feeding both junctions; this biasing condition can model a series dc bias which, as we shall see, is a good approximation of the experimental conditions that we are going to model.

The results obtained by coupling two LJJs with normalized lengths different of 3% to a single small junction are shown in Fig. 3(a); the numerical integration in this case was obtained for the same set of parameters of Fig. 2(a) with the coupling between the long junctions determined by ζ $=0.075$ and identical coupling between each long junction and the small one, i.e., $C_1=C_2$ (and $\zeta=0.008$). Here, as
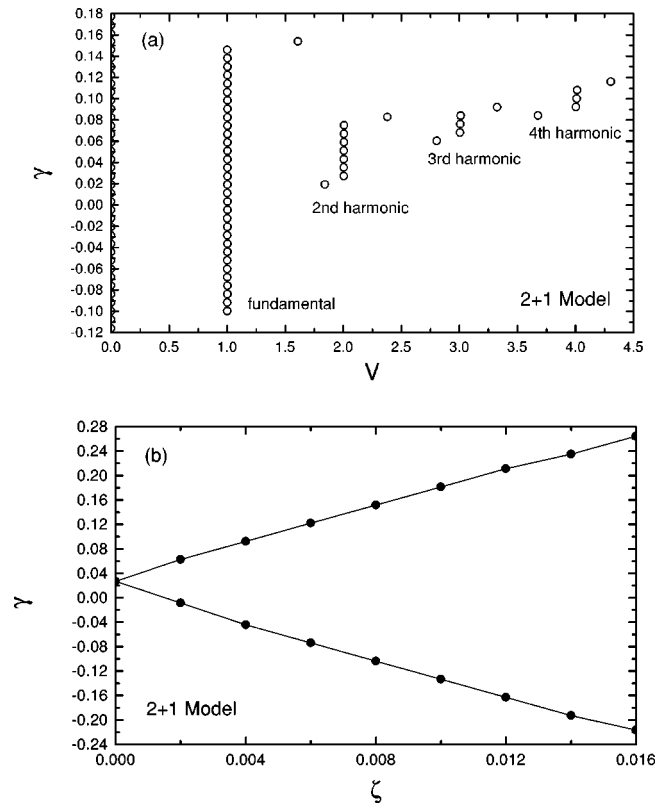

FIG. 3. (a) Current–voltage characteristic of one small junction pumped by two long junctions and (b) dependence of the current amplitude of the highest Shapiro step in (a) upon the coupling parameter, for a fixed value of the bias current $\gamma=0.3$.

before, the points on the zero-voltage axis represent the Josephson current that was depressed in this case of about 25% of its maximum value. We can see that, for the same value of the coupling parameter (between the long and the short junction) the amplitude of the step is larger than in the previous case in which a single long junction is acting as a pumping element.

Although a part of the radiation emitted by a single LJJ is injected in the other long junction and provides the phase locking of the oscillations, there is an evident increase of power feeding the small junction that we estimate to be of the order of 66% at the fundamental frequency of the first Shapiro step. Thus, we conclude that the amplitude of the first phase-locked Shapiro step can be increased by pumping the small junction with two synchronized long junctions. It is worth noting that the phase locking of the two LJJs with different lengths produces a single frequency output: we verified this condition within the limits of the numerical uncertainty. In Fig. 3(b), we show in this case the dependence of the amplitude of the first Shapiro step upon the coupling parameter: the value of the bias current of the LJJs for Fig. 3(b) was $\mathcal{I}^b=0.25$.

Let us consider now the whole system shown in Fig. 1 consisting of two series-connected small junctions and two series-connected long junctions coupled by capacitors. The equations that we have integrated in this case are:

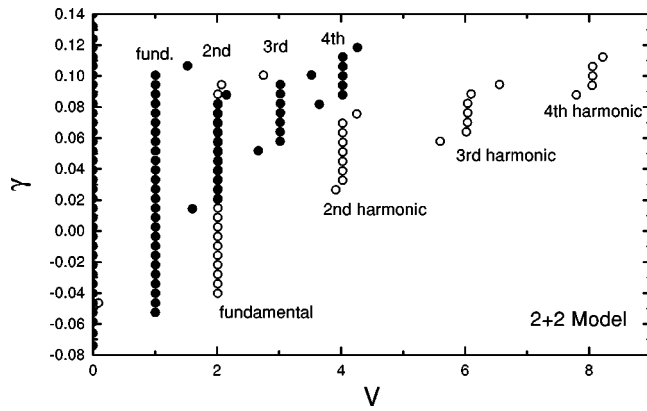$$C_3(\dot{v}_{L1}-\dot{v}_{L2})+C_1(\dot{v}_{L1}-\dot{v}_{s1})=J_{L1}, \tag{8}$$

FIG. 4. Current–voltage characteristic of two small junctions pumped by two coupled long junctions is shown. In order to simulate a series connection of the two small junctions we summed to the voltage of one junction (empty circles) the values obtained from the other (full circles) during the same simulation run. Note that this process generates superposition, the numerical error, in the current interval $0.02 < \gamma < 0.08$ for $V = 2$.

$$C_3(\dot{v}_{L2} - \dot{v}_{L1}) + C_2(\dot{v}_{L2} - \dot{v}_{s2}) = J_{L2}, \qquad (9)$$

$$C_1(\dot{v}_{s1} - \dot{v}_{L1}) = J_{s1}, \qquad (10)$$

$$C_2(\dot{v}_{s2} - \dot{v}_{L2}) = J_{s2}. \qquad (11)$$

Here, as in the system of Eqs. (5)–(7), we have neglected the effect of the inductors connecting the two long junctions and the two small junctions; J_{s1}, J_{s2}, J_{L1}, and J_{L2} can be written as in Eqs. (3) and (4). In Fig. 4, as a result of the series connection the voltages of the small area junctions are summed up and therefore we see two zero crossing steps which correspond to the Shapiro step appearing at the fundamental frequency of the pumping process. Even for Fig. 4, the coupling between the long junctions was characterized by $\zeta = 0.075$ and the coupling between long and small junctions by $C_1 = C_2$ (and $\zeta = 0.008$). As in the previous cases, the voltage output was "monochromatic" within the errors imposed by the numerical integration routine, meaning that the two zero-crossing Shapiro steps of Fig. 4 can be viewed as two steps of a single junction. Here, we have imposed a difference of 3% between the normalized length of the two long junctions.

In Fig. 5, instead we show the dependence of Shapiro steps at the fundamental pumping frequency upon the coupling parameter between long and short junctions for three percentages of difference in length of the junctions: in the figure squares and full circles show the different height of the Shapiro steps at the fundamental frequency in the two small junctions. The value of the coupling parameter between the long junctions increases from a to c. In particular, we have $\zeta = 0.025$, $\zeta = 0.075$, and $\zeta = 0.15$ respectively, for a, b, and c; the results of Figs. 4 and 5 are quite similar to those of Fig. 3 meaning that the simultaneous rf biasing of the two small junctions is very stable and a stable phase locking to the LJJs signal is generated. We also performed simulations in which slightly different parameters for the two small junctions which did not modify significantly the features that we have described so far.
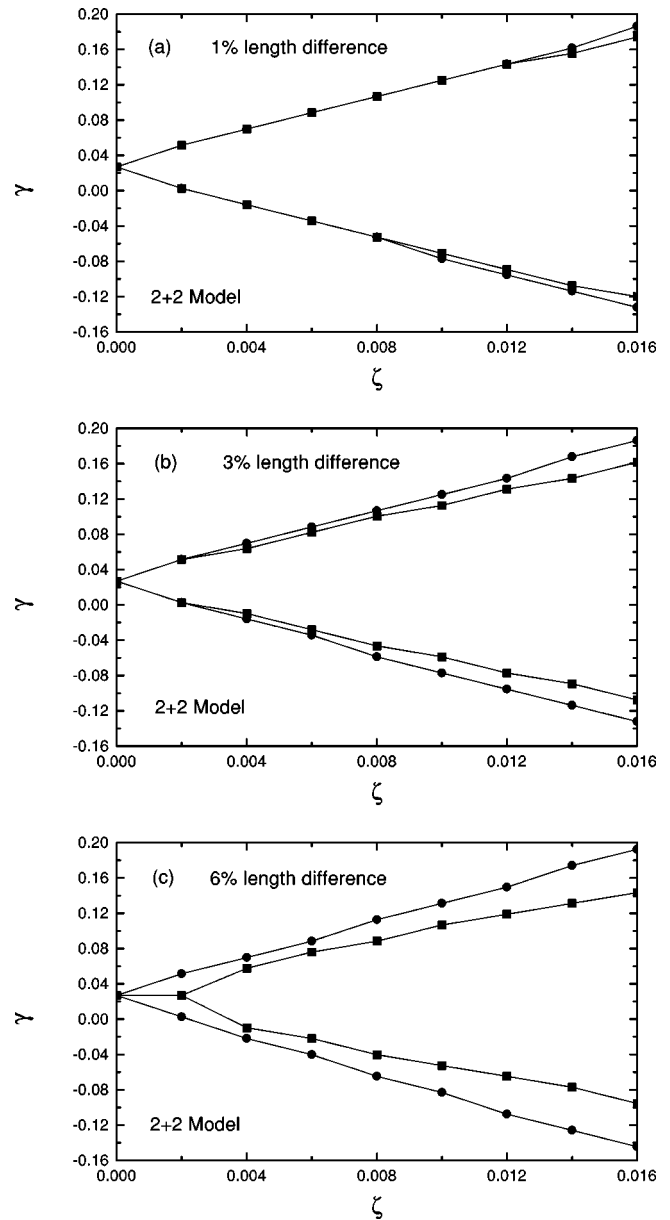

FIG. 5. (a),(b), and (c) show the dependence of the amplitude of the first two Shapiro steps shown in Fig. 4 upon the coupling parameter for three values of percentage length difference between the long junctions.

IV. EXPERIMENTS

A system composed by one LJJ coupled capacitively to a single SJJ (1+1 case) has already been experimentally investigated;[17] measurements on real Josephson junctions were also reported for the (2+1) system, in which two LJJs oscillators are coupled to one SJJ.[18] In both cases, good agreement was found between experimental data and the predictions of the theoretical analysis and simulations; in the (2+1) case in particular, the experiments confirmed an increase of the detected radiation when pumping the SJJ with two coherent oscillators, just like we found in the simulations. However, both in Refs. 17 and 18, the coupling capacitor was obtained adding extra layers to the ones required for the growth of the junctions; the extension of that fabrication
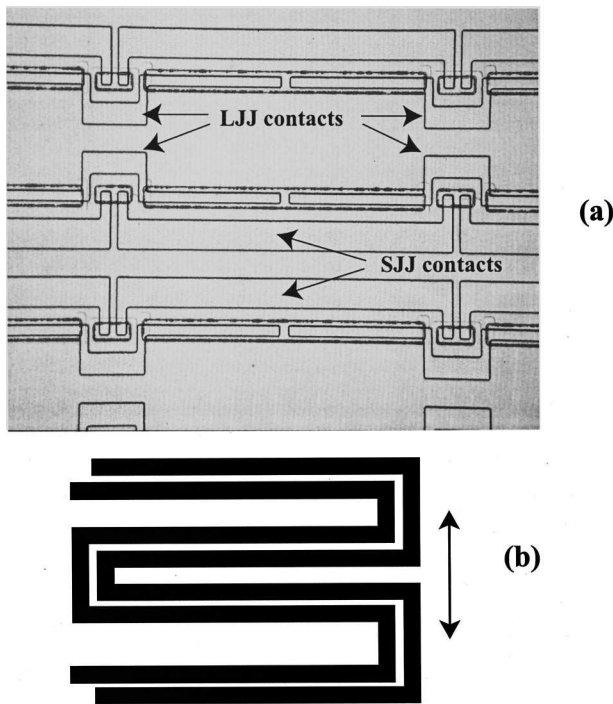
FIG. 6. (a) A photograph of the circuit that we have fabricated showing basic building blocks similar to that of Fig. 1, i.e., two long junctions and two small junctions is shown. The trilayer island where the junctions are located can be clearly identified by the rectangular areas delimited by rougher lines; (b) a sketch of the meander line nesting of the two arrays (each meander line represents the path of a series array). The line by the side indicates the length of the unitary cell of our interdigital capacitor structure.

technique (and coupling concept) to large coupled arrays, an important practical counterpart of our work, would not be easy.

The main problem with the experimental realization of large coupled arrays employing as a basic building block the system studied in the previous section is topological. Since we wanted to keep the configuration of our final layout planar and the fabrication of the circuit compatible with the existing Nb–Al/AlO–Nb trilayer technologies, the design of the system closer to our theoretical modeling was not straightforward. As far as the coupling between the long junctions is concerned, we know that having two ends of the long junctions facing each other may provide by itself a good capacitive connection, very effective for phase locking.[12] The topological constraint arises because we must couple capacitively two series arrays which should be decoupled from the dc point of view without adding extra layers to the trilayer junction fabrication technology. However, since in series connection of junctions we can have only two junctions on the same trilayer island, the basic LJJ building block of our experimental system will be close to the one investigated numerically, i.e., two coupled long junctions.

The samples that we produced were obtained according to a standard PTB Nb trilayer processing.[2] The junctions had a critical current density of 1400 A/cm^2 and a Josephson penetration depth $\lambda_j = 10$ μm. Also, we recall that in this technology, the specific capacitance of the tunnel junctions is $C_s = 3$ μF/cm^2. In Fig. 6(a), we show a detail of the final product of the fabrication process: in the photograph the po-

sition of long and short junctions is clearly visible. We also indicate the Nb contacts connecting the islands where couples of long junctions and couples of short junctions are located. The photo of Fig. 6(a) represents a few sections of a large array whose basic "units" are just two LJJs and two SJJs, just like in our 2+2 system simulations. It is worth noting that we sputtered on the back of the Si wafer a layer of Nb with the intention of using it as a groundplane.

The coupling (and the values of the parameter ζ) between two long junctions on the same Nb island was calculated assuming that the capacitance connecting the LJJs is due to the gap in the striplines. Since the gap separating the two top electrodes of the long junctions is relatively small (there is only a 10 μm distance between the top electrodes), we estimate, using the typical junction parameters of Nb trilayer technology,[19] and the matrix inversion method,[19] a $C_0 \cong 26$ fF and therefore a coupling factor $\zeta = 0.045$. We note that, due to the fact that the trilayer is grown over an oxidized Si substrate which has a groundplane on the back, there exists also a capacitive coupling between the base Nb islands due to the capacitor formed between the top connecting electrode, the Si substrate, and the ground plane. The capacitance of this element, however, is of the order of 0.1 fF which gives $\zeta \cong 10^{-4}$; thus, the coupling between the long junctions on different islands is negligible with respect to the contribution calculated for the junctions on the same island. However, even if it is small, a coupling between the islands containing each two junctions exists.

In order to couple capacitively the two arrays of long and small junctions, we adopted the following strategy. We fabricated two arrays of junctions that each formed a meander-like line: the two meanders formed, respectively, by the series arrays of long and small junctions arrays fit each other as shown in Fig. 6(b). In these conditions, we assume that an interdigital capacitive coupling exists between the two series arrays and that for this coupling the capacitance/unit length is regulated by the equation[20]

$$C_{ul} = \left(\frac{\epsilon_r + 1}{W}\right) L[(n-3)A_1 + A_2]pF/\text{in}, \quad (12)$$

where n is the number of fingers of the interdigital capacitor, L their length in inches, W the total length of the capacitor in inches, and A_1 and A_2 two variables depending on the thickness of the substrate and on the spacing between the fingers. In our case, the dielectric layer is represented by the 0.375 mm thick Si substrate (for Si, we assume $\epsilon_r = 11.4$ at 4.2 K),[21] the length of the fingers is $L = 2.2$ mm and their spacing is of the order of 20 μm. Thus, the coupling is characterized by a capacitance/unit length given by $C_{ul} = (12.4/W)L[(n-3)0.1 + 0.23]pF/\text{in}$. This equation is expected to hold only if the substrate thickness $T > (W/n)$ where W is the total length of the interdigital structure: in our case, since $T = 0.375$ μm, if the length of a unit cell is of the order of 64 μm (to form a unit cell we need a minimal number three fingers), this condition can be expected to hold even if $n = 3$. The capacitance of the unit cell of our inter-digital structure[20] has been evaluated in our case with two

coupled arrays constituted each of 64 junctions. In this case, we get for $W = 64$ μm and $n = 3$ a coupling capacitor of 0.24 pF.

It is worth noting that in our interdigital capacitive modeling we evaluate the overall capacitance coupling the two ports (which are the long and short junction array). Since radiation is distributed all over the stripline of one port (the radiation emitted from the long junctions), we assume that each small junction of the "detector" port will receive the amount of radiation coupled capacitively by the interdigital structure. At the same time, however, each basic cell of the long junction array shall be loaded by the same capacitor (see the circuit model shown in Fig. 1 of Ref. 19) because all the junctions of the two arrays are faced parallel to the ground; more precisely, we have all the junctions capacitances in series to ground with the capacitance of the striplines. We neglect the effect of the junctions capacitances since these are much larger than that of the striplines. The basic limit of our assumptions is the fact that our fingers are "empty," however, considering the frequencies at which our samples are operating (only up to 90 GHz) and that the empty slot in our fingers are only few microns wide, we think that the interdigital capacitive coupling described is a first rough but reasonable approximation. In terms of this modeling, the problem of loading the basic unit of the arrays can be reduced to the $(2+2)$ junction system analyzed in the simulations because all the long junctions of the array are loaded parallel to the interdigital capacitor.

The experimental results that we obtained with the arrays were consistent with the predictions of this model. From the model, we can expect that the coupling will be better for arrays having an increasing number of fingers (n). We can calculate that for $n = 3$, the coupling parameter between two adjacent fingers (i.e., between one double row of long junctions and one double row of small junctions) is $\zeta = 0.15$ which takes us in a region[17] where the reflection of fluxons at the ends of the long junctions and the coupling of electromagnetic radiation to other junctions is just below a threshold value for absorption. This would be a very privileged region in terms of transferring power from a fluxon oscillator to other junctions[17] and we would expect, within the limits of our modeling, radiation-coupling effects. Naturally, increasing the number of fingers we expect more radiation being coupled.

We fabricated several samples and show in Figs. 7, 8, and 9, typical results. Figure 7 shows oscillator on oscillator off current–voltage characteristics of a 64 junctions SJJ array coupled to an array of 64 LJJs (a unit cell in terms of our interdigital capacitor modeling). In order to obtain the emission of radiation, we biased the LJJ array with a current of 600 μA at a voltage of 32 mV. For this sample, the physical extended dimension of the long junctions was 50 μm and the ZFS appeared at asymptotic voltages, in each junction, of 334 μV; thus, at the voltage of 32 mV, we were biased roughly on the 96th ZFS of the long junctions array which makes sense because we had two and sometimes three ZFS for a single junction. We note, however, that in this case, the observed suppression of the Josephson current was of about 40%. This result is consistent with the numerical simulations
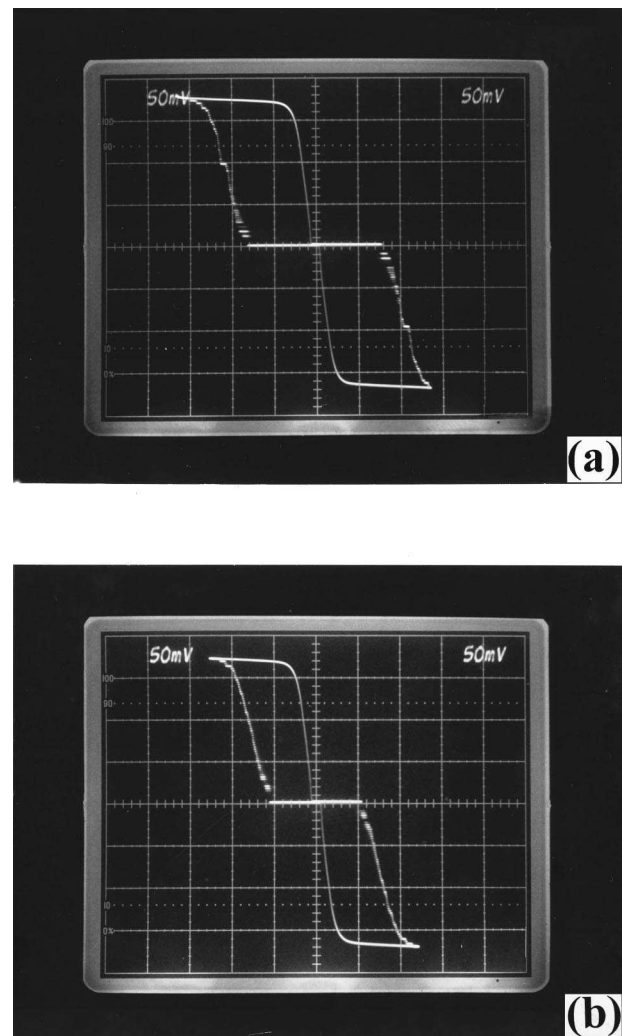

FIG. 7. Oscillators off (a) oscillator on (b) curves for an array of 64 small area junctions coupled to an array of 64 large area junctions are shown. The horizontal (current) scale is 50 μA/div.

because in the experiments we have a coupling parameter $\zeta = 0.15$ which is larger than that $\zeta = 0.008$ value of the simulations which allowed a maximum 25% suppression of the Josephson current.

A result similar to that shown in Fig. 7 was also obtained (see Fig. 8), coupling only eight oscillator junctions to eight detector junctions which were just placed along two parallel lines. In this case, the length of the long junctions and the asymptotic voltages of the ZFSs were the same as for Fig. 7; the bias point of the oscillator array was defined by a current of 600 μA and a voltage of 4.5 mV and therefore we were biased on the 13th ZFS of the array. We see that the relative suppression of the critical currents of the detector array is now of the order of 25%, a result that is not very different from the previous one. As one can expect,[19,20] the coupling provided between the arrays of a unit cell of our interdigital capacitor is of the same order of magnitude of that provided by the coupling of the two microstrips formed by the series arrays. The situation is very different when we increase the number of fingers.

In Fig. 9, we show evidence that our coupling scheme is very effective in transferring power between the two arrays
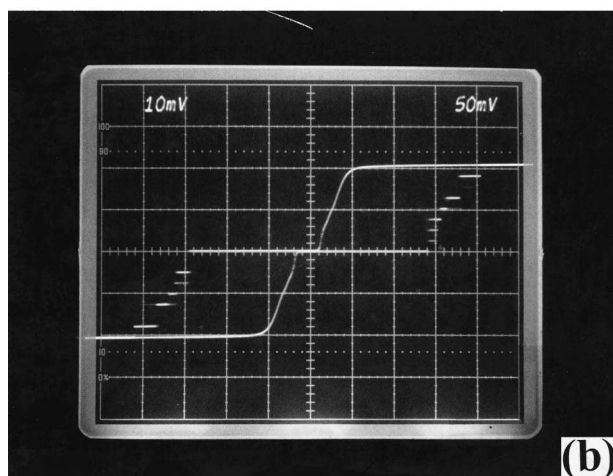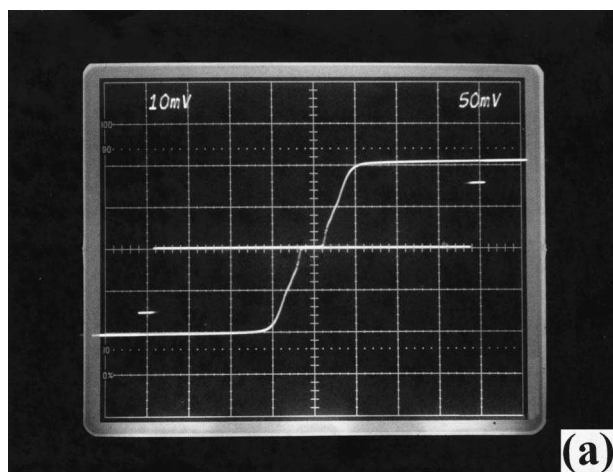
FIG. 8. Oscillator off (a) oscillator on (b) displays for two arrays each containing eight junctions are shown. The horizontal (current) scale is 50 μA/div.
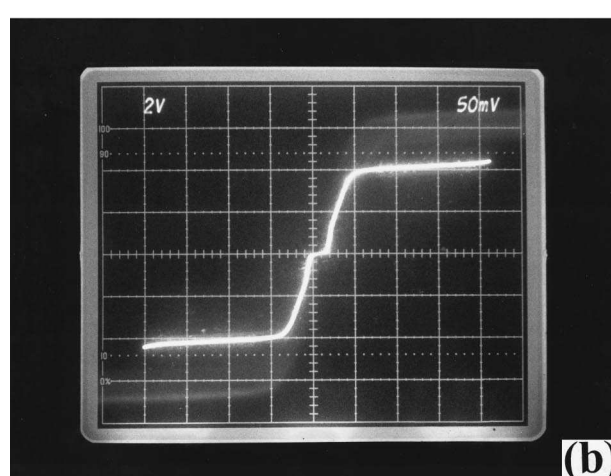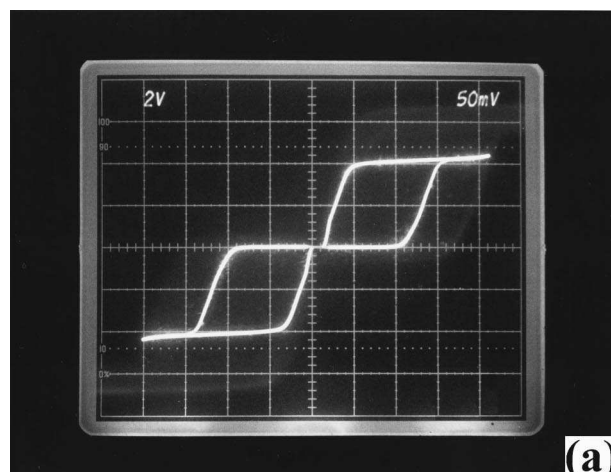
FIG. 9. Oscillator off (a) oscillator on (b) traces for coupled arrays having each 1564 junctions are shown. The horizontal (current) scale is 50 μA/div.

increasing the number of fingers n. In Fig. 9, we see a full depression of the Josephson currents of the array of small junctions. We measured an array of 1564 junctions that was coupled to an array of 1564 LJJs and the number of nested fingers was $n = 47$ for which we estimate a coupling capacitor between the two arrays of the order of 4.9 pF and a coupling factor $\zeta = 3$. We note that in this case, we observed the same coupling of power independently upon the number of biased long junctions: we varied the bias current on the ZFS of the oscillator array in a way that the corresponding voltage would range from few tens up to few hundreds millivolts. This observation leads us to conclude that the coupled power was not a function of the number of biased oscillators but just an effect of the geometrical configuration. The same effect shown in Fig. 9 was measured in several other samples. For the pictures of Fig. 9, we had an oscillator bias current of 380 μA and relative voltage of 80 mV meaning that, since the length of the junctions was the same as before (Figs. 7 and 8), we were biased on the 240th ZFS of the array.

The fact that we observe a full depression of the Josephson current for a coupling factor $\zeta \simeq 3$ is still a factor of

consistency between experiments and numerical simulations because in the simulations we always found that by increasing the coupling parameter, more radiation was transmitted from the long to the short junctions. However, such a high coupling factor would mean an excessive loading of the junctions[17] and the disappearance of the soliton oscillations. This result implies that the modeling in terms of interdigital capacitive coupling needs refinements because in the experiments we always observed very stable ZFS. It is likely that the overall capacitor connecting the two arrays has a value lower than the one we estimated by the interdigital capacitive modeling. Also, as one can see in Figs. 7–9, our arrays had a somewhat high subgap current and it is likely that the coupled electromagnetic power in this voltage region is mostly dissipated resistively. Thus, it was difficult in our case to observe stable Shapiro steps in the subgap regions. These steps were visible at the frequencies expected from the bias point on the oscillator arrays but had a current amplitude of few microamperes. At present, we are fabricating samples that should enable us to improve the quality of the current–voltage characteristics of the junctions, to perform more systematic tests of the interdigital capacitive coupling between

the arrays, and to obtain convincing evidence of the overall coherence of the large number of oscillators.

V. CONCLUSIONS

We have shown numerically that a complicated nonlinear system represented by a coupled array of two long and two short Josephson exhibits remarkable phase-locking properties. The simulations have shown that the power emitted by the large junctions can be used both to synchronize them and to pump small area junctions. From the numerical results, we have also seen that the coherent oscillation gives rise to an increase of the emitted radiation, a phenomenon that has been observed even in the experiments. The stability of the phase locking in the numerical simulations investigated for practical ranges of disuniformities between the junctions is such that applications of our results in the field of metrology and millimeter-wave electronics can be considered. We have reported experimental evidence that the effect found in the simulations due to a capacitive coupling can be observed in arrays shaped in a meander line and nested in an interdigital way. The experiments have shown that radiation can be transmitted from one large oscillator array to a large detector array without affecting the stability of the oscillators and that the coupled electromagnetic power is not dependent on the bias voltage of the oscillators. In these arrays, the basic building block is just represented by the system investigated in the simulations

Our coupling scheme required, in terms of space, for the two arrays each having 1564 junctions, less than 2 mm^2 (excluding the contact pads). This number of junctions is typical for a 1 V standard array chip. Also, the extension to 10 V chips can be easily predicted to occupy less space than the finline antenna of the samples nowadays used for standard maintenance; therefore frequency stabilizer circuits and counters could easily be integrated along with the coupled arrays. The details of these circuits, which are important issues of our research at present, shall be dealt with in a future article. The major advantage of our coupling scheme from the point of view of the rf biasing of large voltage standard arrays (both classical and programmable) is the fact that the electromagnetic power is distributed uniformly all over the junctions. Indeed, any oscillator (semiconductor-based or superconductor-based) whose power is coupled at the input of a finline antenna would not solve the problem of the radiative losses (and subsequent nonuniformity of power distribution) along the arrays. This characteristic might turn out to be especially useful for the SINIS voltage standard technology[22] for which a relatively low amount of micro-

wave power is required: it would not be very difficult to substitute our small junctions array with a SINIS one. Besides these encouraging perspectives for voltage standard purposes, we believe that our radiation transfer scheme could lend itself to other applications in superconducting electronics.

ACKNOWLEDGMENTS

[1] P. Carelli, M. G. Castellano, G. Torrioli, and R. Leoni, Appl. Phys. Lett. **72**, 115 (1998).

[2] J. Kohlman, F. Mueller, P. Gutman, R. Poepel, L. Grimm, F.-W. Duehnschede, W. Meier, and J. Niemeyer, IEEE Trans. Appl. Supercond. **7**, 3411 (1997).

[3] T. Nakamura, K. Enpuku, F. Irie, and Y. Yoshida, J. Appl. Phys. **54**, 3302 (1983); V. P. Koshelets, A. V. Shchukin, S. V. Shitov, and L. V. Filippenko, IEEE Trans. Appl. Supercond. **3**, 2524 (1993); S. V. Shitov, V. P. Koshelets, A. B. Ermakov, L. V. Filippenko, A. M. Barishev, W. Luinge, and Jian-Rong Gao, IEEE Trans. Appl. Supercond. **9**, 3773 (1999).

[4] M. Cirillo, N. Grønbech-Jensen, M. R. Samuelsen, M. Salerno, and G. Verona Rinati, Phys. Rev. B **58**, 12377 (1998).

[5] S. Sakai, A. V. Ustinov, H. Kohlstedt, A. Petraglia, and N. F. Pedersen, Phys. Rev. B **50**, 12905 (1994).

[6] N. Grønbech-Jensen, J. A. Blackburn, and M. R. Samuelsen, Phys. Rev. B **53**, 12364 (1996).

[7] N. F. Pedersen and S. Sakai, Phys. Rev. B **58**, 2820 (1998).

[8] P. A. Booi and S. P. Benz, Appl. Phys. Lett. **68**, 3799 (1996); P. Barbara, A. B. Cawthorne, S. V. Shitov, and C. J. Lobb, Phys. Rev. Lett. **82**, 1963 (1999).

[9] P. Silvestrini, V. G. Palmieri, B. Ruggiero, and M. Russo, Phys. Rev. Lett. **79**, 3046 (1997).

[10] C. Nappi, R. Cristiano, and M. P. Listiskii, Phys. Rev. B **58**, 11685 (1998).

[11] R. L. Kautz, Rep. Prog. Phys. **59**, 935 (1996).

[12] M. Cirillo and F. L. Lloyd, J. Appl. Phys. **61**, 2581 (1987).

[13] R. Monaco, S. Pagano, and G. Costabile, Phys. Lett. A **131**, 122 (1988).

[14] G. Reinisch, J. C. Fernandez, N. Flytzanis, M. Taki, and S. Pnevmatikos, Phys. Rev. B **38**, 11284 (1988).

[15] G. Rotoli, G. Costabile, and R. D. Parmentier, Phys. Rev. B **41**, 1958 (1990).

[16] G. Filatrella, G. Rotoli, N. Grønbech-Jensen, R. D. Parmentier, and N. F. Pedersen, J. Appl. Phys. **72**, 3179 (1992).

[17] M. Cirillo, A. R. Bishop, P. S. Lomdahl, and S. Pace, J. Appl. Phys. **66**, 1772 (1989).

[18] M. Cirillo, I. Modena, F. Santucci, P. Carelli, and R. Leoni, Phys. Lett. A **167**, 175 (1992).

[19] K. C. Gupta, R. Garg, and I. J. Bahl, *Microstrip Lines and Slotlines* (Artech House, Boston, 1979).

[20] G. D. Alley, IEEE Trans. Microwave Theory Tech. **18**, 1028 (1970); Y. M. Zhang, D. Winkler, and T. Claeson, Appl. Phys. Lett. **62**, 3195 (1993).

[21] H. H. Li, J. Phys. Chem. Ref. Data **9**, 561 (1980).

[22] H. Schulze, R. Behr, F. Mueller, and J. Niemeyer, Appl. Phys. Lett. **73**, 996 (1998).